Macromolecules
ARTICLE

Macromolecules **2009**, *42*, 4191–4199 **4191**
DOI: 10.1021/ma900265u

Isothermal Crystallization Behavior of Isotactic Polypropylene H/D Blends as Viewed from Time-Resolved FTIR and Synchrotron SAXS/WAXD Measurements

Kummetha Raghunatha Reddy,[†] Kohji Tashiro,*[,†] Takashi Sakurai,[‡] Noboru Yamaguchi,[‡] Sono Sasaki,[§] Hiroyasu Masunaga,[§] and Masaki Takata[§]

[†]*Department of Future Industry-oriented Basic Science and Materials, Toyota Technological Institute, Tempaku, Nagoya 468-8511, Japan,* [‡]*Petrochemicals Research Laboratory, Sumitomo Chemical Co. Ltd. Kitasode, Sodegaura, Chiba 299-0295, Japan, and* [§]*Japan Synchrotron Radiation Research Institute (JASRI), Sayo-gun, Hyogo, 679-5198, Japan.*

Received February 5, 2009; Revised Manuscript Received April 22, 2009

ABSTRACT: The melt isothermal crystallization behavior has been investigated for a series of blend samples of deuterated (D) and hydrogenated (H) species of isotactic polypropylene by means of time-resolved Fourier transform infrared (FTIR) spectral measurement and simultaneous small-angle X-ray scattering (SAXS)/wide-angle X-ray diffraction (WAXD) measurements using synchrotron radiation source in SPring-8. The SAXS data collected were analyzed in the three different time regions. The Guinier plot in the early stage of crystallization gave the average size of isolated domains formed in the melt. In the middle stage, the correlation between these domains was analyzed using the Debye−Bueche equation. In the later stage of crystallization, the correlation function was calculated to estimate the degree of crystallinity and the long period of the stacked lamellae. The IR data analysis clarified the formation process of regular helical chains in the isothermal crystallization phenomenon. The combination of FTIR, WAXD, and SAXS data has revealed a concrete structural evolution process as follows: (i) In the early stage, the short helices start to be formed, and they gather together to create an isolated domain of about 330 Å radius of gyration. (ii) The domain size decreases gradually to about 300 Å, and (iii) these domains start to have some weak correlation to each other with ca. 300 Å correlation length. (iv) In these domains, the regular chain segments grow to longer helices, and the correlation distance becomes shorter to ca. 200 Å, and finally, (v) the stacked lamellae with long period of ca. 200 Å are formed and stabilized. The crystallization behavior of the D/H 50/50 blend sample was also investigated, and the origin of cocrystallization phenomenon has been discussed.

Introduction

Isotactic polypropylene (iPP) is one of the most basically important polymers from both industrial and scientific points of view. Among the various characteristic features of iPP, the structural change occurring in the crystallization from the melt is a significant research theme because the mechanical properties of iPP are controlled by the aggregation structure of crystalline and amorphous phases or the higher-order structure.[1,2] So far, many papers have been reported that try to describe the structural evolution process in the crystallization process of iPP through the investigation by X-ray scattering,[3] transmission electron microscope (TEM),[4] differential scanning calorimeter (DSC),[5] Fourier transform infrared (FTIR) and Raman spectroscopy,[6−8] small-angle light scattering (SALS),[9] and so on. But a deeper understanding is needed to reveal the details of the structural growth by viewing the phenomena from the various scales during the rapidly occurring crystallization process.[10]

The crystallization of iPP is complex because the various different crystalline modifications (α, β, and γ) appear in the crystallization depending on the conditions and affect the morphologies of the higher order structure sensitively.[11−15] As an idea to know the detailed behavior of individual chains in the crystallization process, we have been studying the crystallization of a series of blend samples between the deuterated (D) and hydrogenated (H) chains. Because of the difference in vibrational frequency[16−18] (and neutron scattering length[19,20]) between these two species, we can trace the behavior of chains by monitoring the infrared spectral change. This idea was applied to the case of polyethylene.[16−28] In the case of iPP, only a limited number of papers were reported that utilize the D and H blend samples.[29−32] Before we utilize these blend samples, we need to check an occurrence of the cocrystallization phenomenon between the D and H species. If not, the phase separation occurs between these two species, and the starting principle is broken.[22−28] In a previous paper,[33] by analyzing the DSC and infrared spectral data in detail, we successfully established the cocrystallization phenomenon between the H and D species of iPP.

Once the cocrystallization concept was established, we applied the D/H blend samples to the study of the isothermal crystallization process of iPP. We found that the crystallization rate is higher for the blend sample with higher D content.[34] To understand the phenomenon, we need to investigate the formation mechanism of higher-order structure in the isothermal crystallization process from the melt. For this purpose, the simultaneous time-resolved small-angle X-ray scattering (SAXS) and wide-angle X-ray diffraction (WAXD) measurements using a synchrotron X-ray radiation may be the best way. We can quantitatively know the growth of nuclei and the stacked lamellae formation by analyzing the SAXS data. The WAXD data tell us the growth of the crystal lattice.

*Corresponding author. E-mail: ktashiro@toyota-ti.ac.jp.

Published on Web 05/19/2009

In addition to the SAXS/WAXD measurements, we need to collect the vibrational spectroscopic data to know the formation process of regular helical segments because the vibrational spectroscopic method is one of the strongest weapons for tracing the conformational change in the crystallization phenomenon. We can utilize much literature about the characteristic IR bands that are useful for the identification of concrete conformation and aggregation structure of iPP chains.[6−8,35,36] For the study of structural change, a concept of the critical sequence length is useful.[37−43] There might be many infrared bands that are sensitive to the crystallinity. This sensitivity is not always the same, but each band has its own characteristic "critical sequence length". For example, in the process of conformational regularization of a chain, some bands might be detected in a stage of short helix formation, but other bands might appear for the first time when the helix grows to appreciable length. The critical number of monomeric units included in the helical segment of a certain length is called the critical sequence length, beyond which the infrared band can be detected for the first time.[37−43] The critical sequence lengths were evaluated concretely on the basis of "isotope dilution technique" in which a series of random copolymers consisting of deuterated and hydrogenated monomeric units were used to measure the infrared spectra.[39] Because the deuterated and hydrogenated monomeric units vibrate at appreciably different frequencies, no vibrational coupling is expected to occur in an approximation. Therefore, the vibrational coupling occurs only in the segments of a finite number of D (or H) units, and the vibrational amplitude is dependent on this sequence length. In other words, the vibrational coupling can be made for the first time when the D (or H) monomeric units form a regular helix of some critical length, and then the corresponding infrared band can be detected in the spectrum. Because the different bands may have different critical sequence lengths, the detection of time gap between the two bands of different critical sequence lengths allows us to speculate that the helix grows longer during this time gap. This idea can be applied to the study of helical regularization phenomenon in the crystallization process: for example, the solvent-induced crystallization of syndiotactic polystyrene,[44] the order−disorder transition of orthorhombic polyethylene,[45] and the ferroelectric phase transition of vinylidene fluoride−trifluoroethylene copolymers.[46] Also, in the case of iPP, the critical sequence lengths were estimated for some bands. The minimum "*m*" values for different infrared at 973, 998, 841, and 1220 cm^{-1} of iPP are 5, 10, 12, and 15 monomer units in the helical sequences.[37−43] Zhu et al. used these bands for the study of the conformational regularization process of iPP in the isothermal crystallization of the pure H sample,[37] but they did not correlate this information to the formation of a higher-order structure.

In the first half of the present article, we will investigate the structural evolution process from the various levels by combining the IR, SAXS, and WAXD data to clarify the relationship between the conformational change of molecules and the formation of crystal lattice and the growth of crystallize lamellae. It should be noticed here that the comparison of the experimental data among the IR, SAXS, and WAXD methods can be made under such an assumption that the sensitivities of these different methods are essentially the same for the same phenomenon. There might be two types of meaning in the discussion of sensitivity. (a) One is a so-called sensitivity, that is, to what extent a weak signal can be detected that is distinguishable from the noise, and (b) the IR and X-ray can detect different information about the structure. The IR is sensitive to local molecular structure, whereas the X-ray is sensitive to the aggregation of molecules when we study the solid state of a material. The sensitivity (a) or higher signal-to-noise ratio is also dependent on the volume of sample, which is different between IR (thin film) and X-ray (thicker film). Even when we use a single sample and measure the IR and X-ray data simultaneously, it is difficult, strictly speaking, to compare the starting point of detection of the IR and X-ray signals because of these two factors (a) and (b). This is a quite important but very difficult theme in all material science that uses the pair of vibrational spectroscopic and X-ray methods, and it should be challenged. In the present time, we would like to say that "the comparison of the IR and X-ray data is made under the assumption of almost the same sensitivity" in the present article.

As mentioned in the earlier paragraphs, the D/H blend samples of iPP show almost perfect cocrystallization, even when crystallized slowly from the melt.[33] However, the kinetic study of thermal data revealed that the crystallization rate is different between the pure D and H species. More significantly, the crystallization rate continuously changes depending on the D/H content.[34] Why must the D and H components of originally different crystallization rates be cocrystallized in the cooling process from the melt ? An answer might be in this way: The diffusion rates of the D and H chains affect each other by intermolecular interactions, and they migrate to the front site of the growing lamella at the same time. If the isotopic fractionation occurs, then the H (or D) chains escape from the aggregation of D and H chains in the melt and form the cluster at first. Therefore, we do not have a perfectly cocrystallized lamella any more. In other words, such an isotopic fractionation does not occur because we actually know the experimental data showing the almost perfect cocrystallization phenomenon for any pair of iPP D/H blends. The FT-IR data obtained in the temperature jump experiment may give us any indication about this problem. In the second half of this article, the FTIR, SAXS, and WAXD data collected for the D/H blend samples are also analyzed in detail to clarify the origin of the cocrystallization phenomenon of the D and H species.

Experimental Section

Samples. As described in the previous papers,[33,34] the D and H iPP samples were synthesized by polymerizing the deuterated and hydrogenated propene monomers using a metallocene catalyst system. The characterizations of results of these samples are shown in Table 1. The tacticity of these samples was estimated to be about 0.99 (mmmm). We prepared the blend samples by dissolving the H and D species in 50/50 molar ratio in boiling *p*-xylene at 2 wt % and by precipitating into methanol. The samples were dried in vacuo at 100 °C overnight and cooled to room temperature. The molecular weight distributions of the samples used are not very narrow. The experimental analysis would contain some ambiguity about the crystallization rate and so on, but we would proceed the discussion by taking this point into consideration. To erase air bubbles contained in the samples, which may give strong diffuse scattering in the SAXS experiment, the samples were heated to 200 °C in a vacuum oven and kept for 5 h, followed by slow cooling to room temperature.[10,47]

Measurements *Simultaneous Measurement of Synchrotron Small-Angle X-ray Scattering and Wide-Angle X-ray Diffraction*. A sample was packed to a small metal holder and set in temperature jump equipment. In the isothermal crystallization experiment, the temperature must be changed as quickly as possible from above the melting point to the predetermined temperature (T_c). As illustrated in Figure 1, the temperature

Table 1. Characterization of iPP Samples

sample	M_w	M_w/M_n
hydrogenated iPP	160 000	3.0
deuterated iPP	200 000	2.5

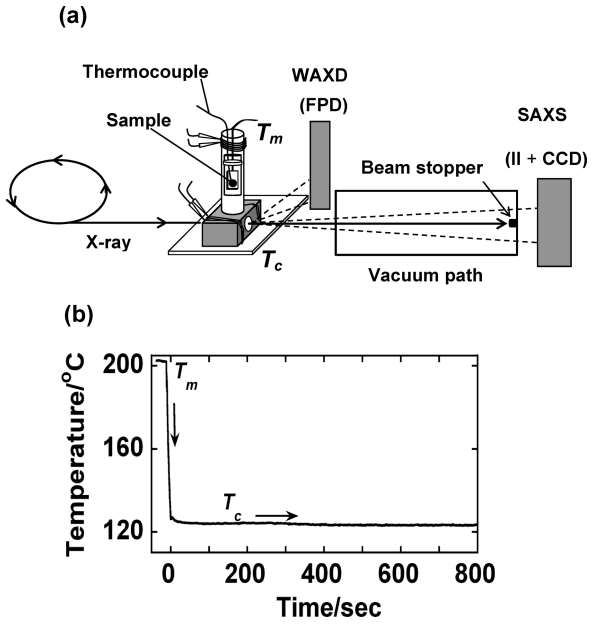

Figure 1. Schematic illustrations of (a) the simultaneous SAXS/WAXD measurement system and (b) the temperature jump profile in the SAXS/WAXD experiment.

jump cell contains two chambers. One chamber was maintained at the melt temperature (T_m = 200 °C), and the other chamber was maintained at the crystallization temperature T_c. The T_c was chosen so that the ΔT or the degree of super cooling was equal for the various D/H blends by referring to the equilibrium melting points evaluated for these samples. (See Table 2.)[34] After staying 8−10 min in the melt to erase all of the thermal histories, the sample cell was rapidly transferred to another chamber maintained at T_c. During the transfer of the sample cell, air was blown on the sample holder to achieve the T_c rapidly (ca. 700 °C/min). The details of the temperature jump equipment are described elsewhere.[10,47] We monitored the actual sample temperature by inserting a thermocouple into the sample. During the isothermal crystallization measurements, the temperature fluctuations were less than ± 0.5 °C.

The simultaneous SAXS and WAXD measurements were performed in the BL40B2 beamline (wavelength λ = 1.0 Å) at SPring-8, Japan. The camera lengths for the SAXS and WAXD measurements were set to about 2250 and 100 mm, respectively. A dried chicken leg tendon collagen and cerium oxide powder were used as the standard references for the camera distance corrections of SAXS and WAXD, respectively. The 2D SAXS and WAXD profiles were detected with a CCD (Hamamatsu Photonics, C4880) with X-ray imaging intensifier (IV4554P, Hamamatsu Photonics) and a CMOS FP detector (C9728DK, Hamamatsu Photonics, Japan), respectively. The SAXS and WAXD data were collected at an interval of 2 to 3 s. The 2D SAXS and WAXD were corrected for the background scatterings. We obtained the 1D SAXS profiles by circularly integrating the 2D data as a function of scattering vector, q, where $q = (4\pi/\lambda) \sin\theta$, and 2θ is a scattering angle and λ is an incident X-ray wavelength.

Time-Resolved Fourier Transform Infrared Measurements. The heating chamber for the IR experiment used in the present study was the same as that used in the previous research.[10,27] A homogeneous mixture of KBr and iPP powders was prepared as a disk, which was fixed to a metal holder, and a thermocouple was embedded to monitor the sample temperature directly. The holder was heated above 200 °C for 8−10 min to erase the thermal history. Then, it was transferred to another heater by a magnetic relay system, and the sample was maintained at a predetermined crystallization temperature (T_c), during which the time-resolved FTIR measurements were performed at a time

Table 2. T_m^o Values for a Series of D/H Blend Samples

samples	T_m^o (°C)
H100	196.5
H75	194.6
H50	192.3
H25	189.2
H0	187.5

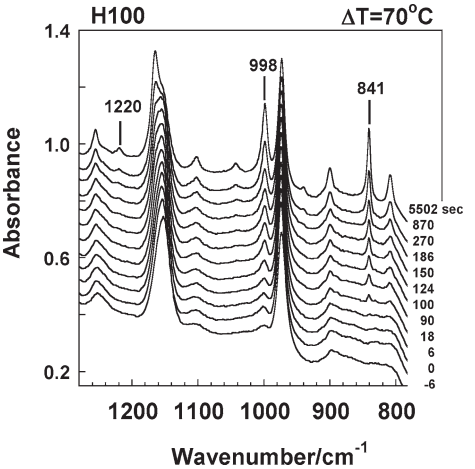

Figure 2. Time dependence of infrared spectra measured for iPP H100 sample at ΔT = 70 °C in the isothermal crystallization process from the melt.

interval of 3 s. The FTIR spectra were collected at 2 cm^{-1} resolution power using a Varian FTS7000 rapid-scan-type FTIR spectrometer equipped with an MCT detector in the transmission mode. We estimated the integrated intensity of an IR band by separating the spectrum into the components by using the commercial software Grams (Thermo Electron). It should be noted here that the temperature jump rate (ca. 700 °C/min) was essentially the same as that attained in the X-ray scattering experiment, as checked by a thermocouple that was embedded into a sample to monitor the sample temperature directly for these two experiments.[10,27,28] This situation has allowed us to compare the data of these two different experiments (of course, under the assumption of the same sensitivity as mentioned above).

Results and Discussion

Crystallization of H100 *Time Dependence of Infrared Spectra.* The crystallization rate is sensitively influenced by the degree of supercooling (ΔT), which is the difference between the equilibrium melting temperature (T_m^o) and the crystallization temperature (T_c): $\Delta T = T_m^o - T_c$. The T_m^o values were evaluated for a series of blend samples on the basis of the Hoffmann−Week plot, as reported in the previous paper.[34] In Table 2, the T_m^o are listed. Figure 2 shows the time dependence of infrared spectra measured for the pure H100 sample in the isothermal crystallization process at ΔT = 70 °C. Figure 3 shows the time dependence of normalized integrated intensity estimated for several bands. The band at 975 cm^{-1} comes from the amorphous phase and started to decrease gradually with time. The time of detection of the crystallization-sensitive band is different. For example, the band at 998 cm^{-1} started to increase in intensity at around 20 s after the temperature reached the T_c. The 841 cm^{-1} band was detected at ca. 30 s. Another band at 1220 cm^{-1} appeared after ca. 80 s. These bands have the critical sequence length, m, of 10, 14, and longer than 15 monomeric units, respectively.[37−43] Therefore, it may be said that the short helical segments that consist of 10−14 monomer units start to be formed after the start of crystallization. The bands with longer helical sequence length, 841 (m = 10−12)

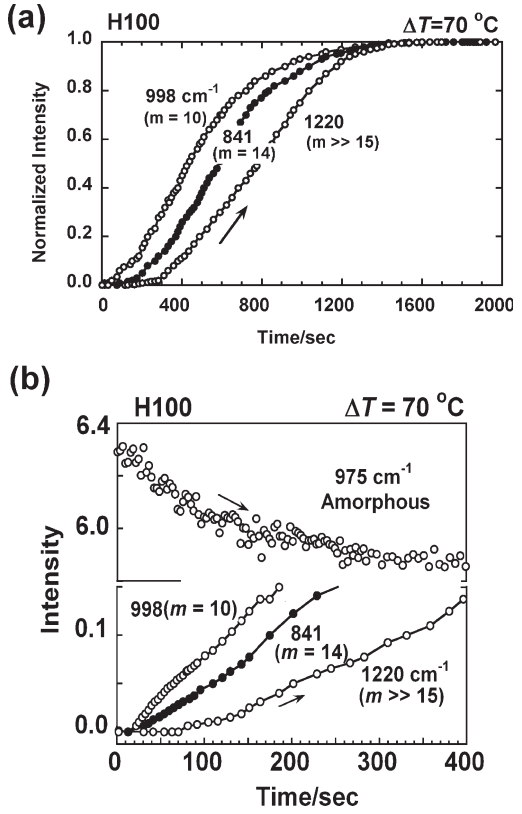

Figure 3. (a) Time dependence of the integrated intensity of the various infrared bands estimated for iPP H100 sample in a wide time region (ΔT = 70 °C, refer to Figure 2). (b) The zooming up of the early stage of crystallization.

and 1220 cm^{-1} ($m \gg 15$), appear at a much later time, indicating that the short helices grow to longer helices in the crystallization process. This helical chain evolution is essentially the same as that reported by Zhu et al.,[6] although the details of their temperature jump experiment are not known.

Time-Resolved Synchrotron Small-Angle X-ray Scattering/Wide-Angle X-ray Diffraction Measurements. Figure 4a,b shows the time dependence of SAXS and WAXD profiles of the H100 sample, respectively, measured at ΔT = 70 °C or the same degree of supercooling as that of the IR experiment. In Figure 4a, the SAXS component due to the molten state was erased, and only the SAXS component coming from the stacked lamellar structure is plotted to emphasize the evolution of the stacked lamellar structure and to estimate the invariant Q based on this structure. In the later stage of crystallization the long period peak appeared in the SAXS profile after some induction period. In the WAXD pattern, as the time passed, the intensity of the amorphous halo decreased, and the crystalline peaks appeared where the peaks of α and γ forms were detected together.[34] Figure 5a,b shows the time dependences of the normalized invariant Q estimated from the SAXS data and the normalized degree of crystallinity from the WAXD data at ΔT = 70 °C. The invariant Q was estimated on the basis of SAXS data by the calculation of the correlation function, as explained in a later section. The crystallinity, X_c, was evaluated as the ratio of the integrated intensities of crystalline peaks to the total area observed in Figure 4b. The Q and X_c values increased with time in essentially the same manner.

Figure 6 shows the observed SAXS profiles ($I(q)$ vs q) detected in the earlier time region immediately after the temperature jump, where the SAXS patterns were corrected only for the background scattering from the air and

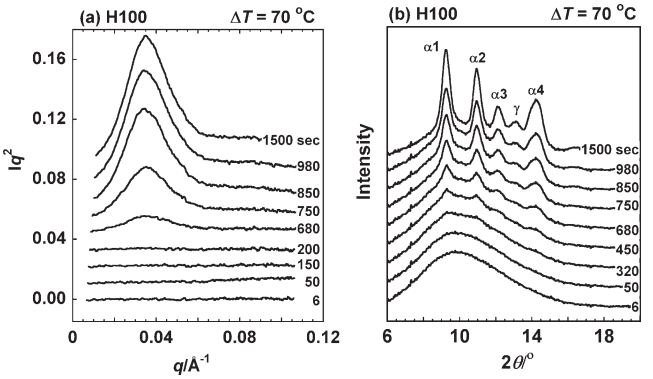

Figure 4. (a) SAXS and (b) WAXD developments during the isothermal crystallization of H100 sample. The WAXD data are presented in 2θ (λ = 1.00 Å), and the reflection peaks are indexed as α1 (110), α2 (040), α3(130), α4 (111), (131), and γ (117) for the α_1 and γ crystal forms, respectively.

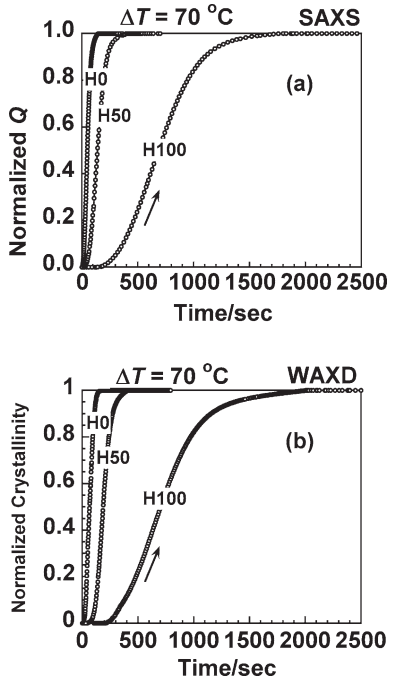

Figure 5. Time dependence of the normalized invariant, Q, and the crystallinity estimated for H0, H50, and H100 samples by the SAXS and WAXD data, respectively.

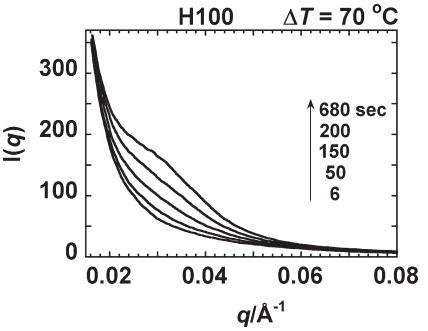

Figure 6. Time dependence of SAXS profiles measured in the early stage of isothermal crystallization of H100 sample at ΔT = 70 °C.

temperature jump cell. (Refer to Figure 4a.) Here we imagine not unreasonably that the density fluctuation may occur in the melt, and some denser regions start to grow to form domains, but these domains are isolated from each other.

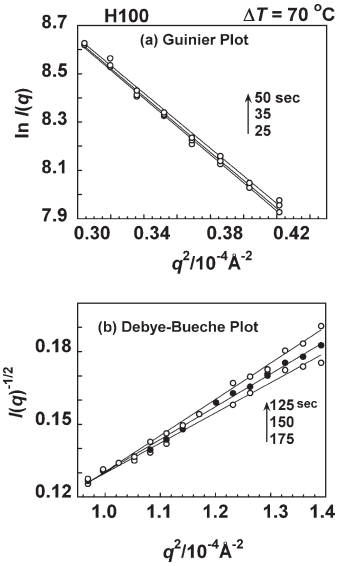

Figure 7. Some examples of (a) Guinier plot and (b) Debye−Bueche plot in the early stage of isothermal crystallization of H100 samples.

After the passage of a certain amount of time, these domains gather together, and finally, a stacked lamellar structure may be formed from these domains. To check this natural structure evolution, we analyzed the SAXS data on the basis of (i) the Guinier plot in the earlier time region where isolated domains are formed, (ii) the Debye−Bueche plot in the time region where the correlation of the two domains becomes stronger, and (iii) the correlation function in the later stage to estimate the stacked lamellar structure.

Guinier Plot for an Isolated Domain. The intensity variation is given by[48−50]

$$\ln[I(q)] = \ln[I(0)] - q^2 R_g^2/3 \quad (1)$$

where R_g is the radius of gyration to represent an isolated domain's size. In the present case, we used the q range < 0.01 Å^{-1} by referring to the radius of gyration that is expected for a single chain.[51] Figure 7a shows some examples of Guinier plot.

Debye−Bueche Plots for the Two-Phase Structure. This model is based on a biphasic system where the refractive indices of these two phases have relatively close values. These two phases may be combined with a sharp interphase. The correlation between the neighboring domains separated at distance z is given by $\Gamma(z) = e^{-z/\xi}$, and the corresponding scattering intensity, $I(q)$, is expressed by eq 2[52]

$$1/I(q) = [1/A + (\xi^2/A)q^2]^2 \quad (2)$$

where A is a constant and ξ is a correlation length. From the plots $I(q)^{-1/2}$ versus q^2, we can obtain the ξ as a ratio of the slope and intercept of straight line. Figure 7b shows some examples of the Debye−Bueche plot. In Figure 8, the R_g of isolated domains obtained by Guinier plot and the correlation length (ξ) estimated by Debye−Bueche plot are shown as a function of time at $\Delta T = 70$ °C. The R_g is about 330 Å in the initial stage of isothermal crystallization. As the time passes, the R_g decreases almost linearly. This R_g is related to the Debye−Bueche correlation length, ξ, of ca. 300 Å at around 100 s. This means that the domains cannot be assumed any more to be isolated, but some correlation starts to occur. The reason why this happened after about 100 s comes from the infrared data, as will be discussed in a later section.

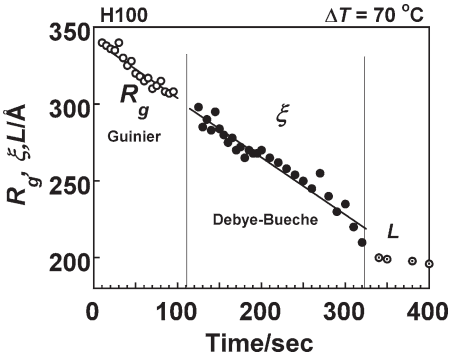

Figure 8. Time evolution of domain size (R_g) and correlation length (ξ) of H100 sample estimated from Guinier and Debye−Bueche plots, respectively. The long period, L, estimated in a later stage of crystallization is also shown for comparison.

Correlation Function for Lamellar Structure. As seen in Figure 8, at around 280 s, the ξ value started to deviate from the linear relation and approach the value of long period, L, estimated for the stacked lamellae structure model. In this region, the invariant Q started to increase remarkably. The structural parameters of the stacked lamellae are estimated using the 1D electron density correlation function $K(z)$. Under the assumption of the two-phase model consisting of the alternatively stacked crystalline and amorphous layers (Figure 9), the $K(z)$ is defined by the following equation[53]

$$K(z) = <[\eta(z') - <\eta>][\eta(z+z') - <\eta>]> = 2\int_0^\infty (\pi)^{-1} q^2 I(q)\cos(qz)\,dq \quad (3)$$

where $< >$ is the statistical average and $\eta(z)$ and $<\eta>$ are the electron density variation along the lamellar normal and the mean electron density, respectively. In this equation, the intensity, $I(q)$, given in Figure 4a is used because the correlation function of the stacked lamellar structure is calculated here. As indicated in Figure 9a, the various points on the $K(z)$ curve give the various structural parameters: the invariant, Q, the mean lamellar thickness, $<d>$, the mean transition zone thickness, d_{tr}, the mean core thickness, d_o and the long period, L. Figure 9b shows the time evolution of $K(z)$ calculated for the H100 sample at $\Delta T = 70$ °C. Figure 10 shows the time dependence of these structural parameters obtained for the H100 sample in the later stage of crystallization. Parallel to an increase in Q, the long period peak started to be detected and increased its intensity, whereas the long period itself decreased in value. The lamellar thickness increased at the beginning of crystallization and saturated.

Structural Evolution Process. These infrared spectral data are combined with the SAXS/WAXD data, as shown in Figure 11, by focusing on the early stage of isothermal crystallization. This comparison can be made reasonably because the temperature jump process was essentially the same between these two independent experiments ($\Delta T = 70$ °C). After the sample temperature reached the T_c at 0 s, the amorphous band at 975 cm^{-1} decreased in intensity. The helical bands at 998, 841, and 1220 cm^{-1} started to appear at around 20, 30, and 80 s, respectively. In this Figure, the half-width of the amorphous band is also shown. The half-width reflects the degree of conformational distribution in the amorphous phase and also the thermal mobility of the molecular chains.[54] If the regularization occurs in the amorphous or the melt state, then the amorphous chains are subjected to some constraints because of the existence of these regular parts, making the thermal

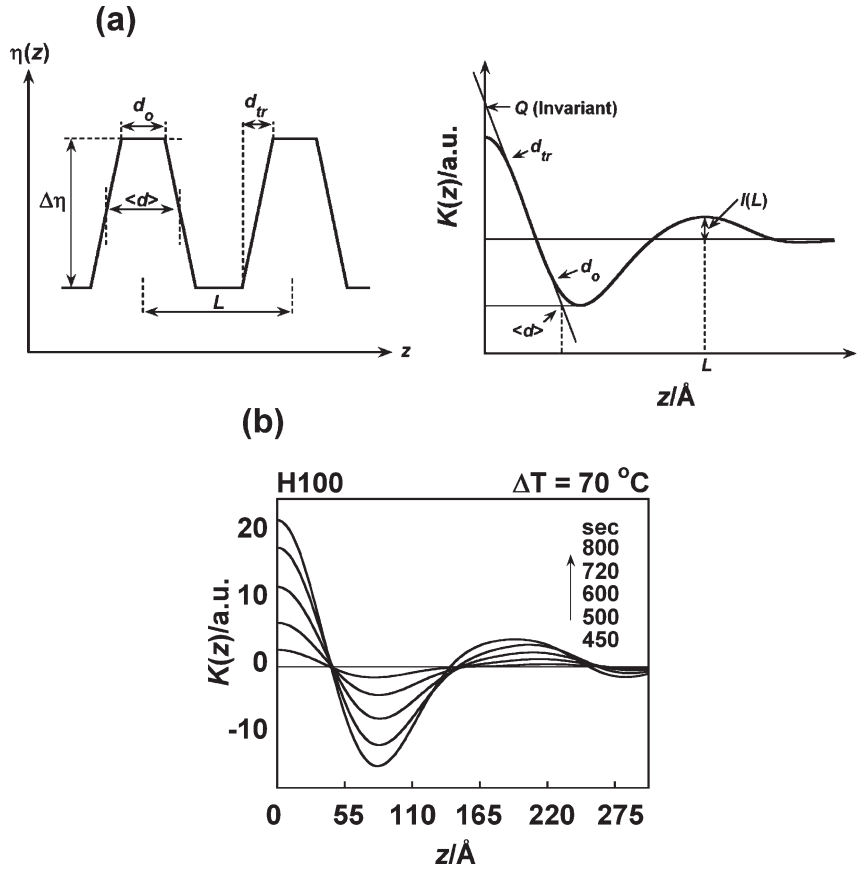

Figure 9. (a) Model of 1D electron density distribution in the lamellar system and the corresponding electron density correlation function $K(z)$. Q: the invariant, d_{tr}: thickness of transition zone between the crystalline lamella and amorphous part, d_o: thickness of core lamella, $<d>$: mean lamella thickness, L: long period, and $I(L)$ is the scattering intensity. (b) Time evolution of $K(z)$ calculated for H100 sample.

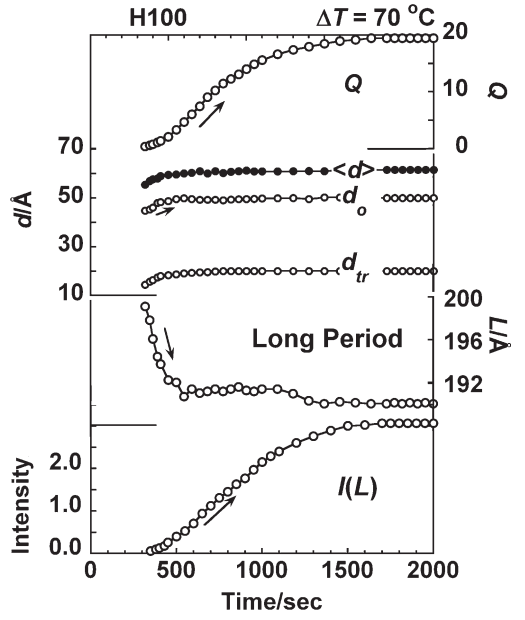

Figure 10. Evolution of various structural parameters of H100 sample plotted as a function of time as obtained by the calculation of correlation function. (Refer to Figure 9.)

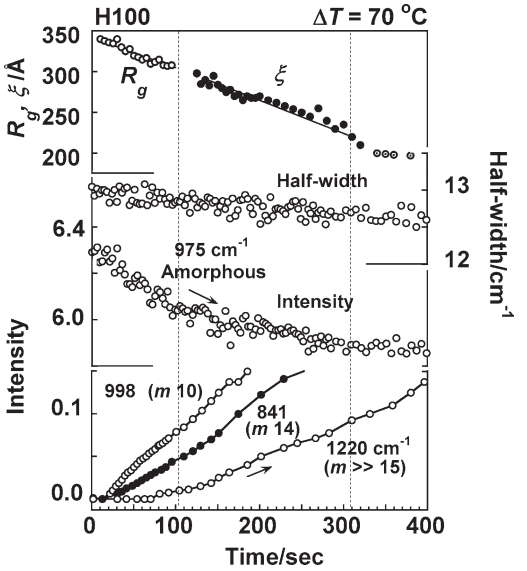

Figure 11. Time dependences of the radius of gyration (R_g) and correlation length (ξ) evaluated from the SAXS data analysis and the integrated intensity of the infrared bands with different critical sequence length. The half-width and intensity of the amorphous band is also plotted here.

motion slower. At the same time, some change in conformational distribution may also occur. In this time region, the half-width is observed to change only slightly. The motion and conformational distribution in the amorphous part are not affected very much by the regularization of helical domains at such a high temperature of T_c = 127 °C.

The R_g gradually decreases parallel to the appearance of regular helices and their growth. In the time region of ca. 100 s, the R_g value smoothly fits the ξ, just around 100 s, when the longer helices start to appear, as represented by the 1220 cm^{-1} band. The ξ value decreases almost linearly and starts to deviate from the linear line at about 300 s. This

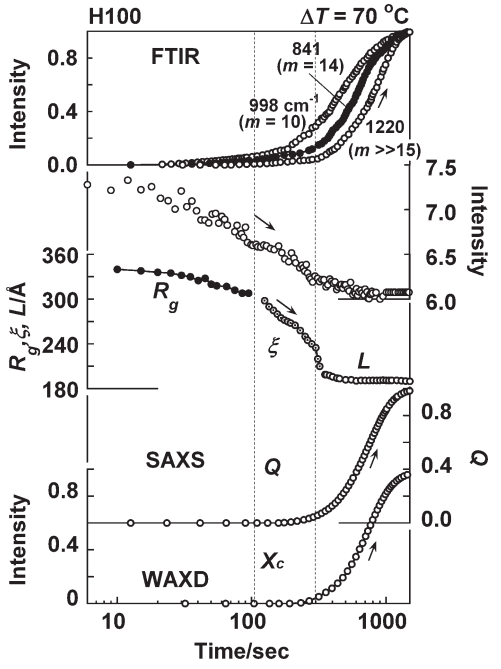

Figure 12. Comparison of infrared band intensity changes with the SAXS (invariant Q) and WAXD (degree of crystallinity) and the long period estimated in the isothermal crystallization process of iPP H100 sample (ΔT = 70 °C).

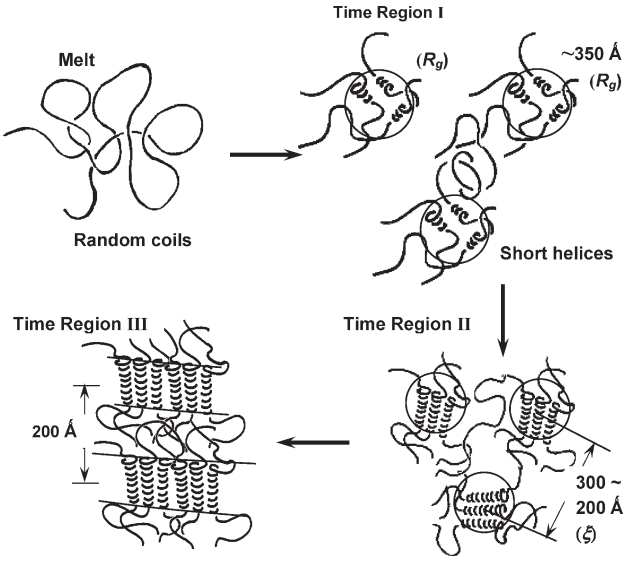

Figure 13. Schematic illustrations of structural evolution process occurring in the isothermal crystallization process of iPP H100 sample.

situation is emphasized in Figure 12, where the time dependence of the invariant Q, estimated by SAXS analysis, and the degree of crystallinity, X_c, estimated from the WAXD data, are compared with the IR data. The time of 300 s is important because the crystal lamellae start to appear, as noticed from the increasing crystallinity, X_c, and invariant, Q, representing the total amount of crystal lattice of the α_1 form. (The γ form also starts to appear at almost the same time.) The infrared band intensity of long helices also steeply increases around this time region.

In this way the combination of the various information obtained from the infrared and SAXS/WAXD data allows us to deduce the structural evolution process of the iPP H100 sample in the isothermal crystallization at ΔT = 70 °C, as illustrated in Figure 13. In the early stage of crystallization,

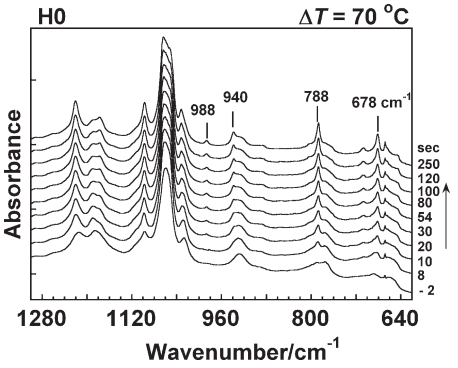

Figure 14. Time dependence of infrared spectra measured in the isothermal crystallization process of iPP H0 (pure D) sample at ΔT = 70 °C.

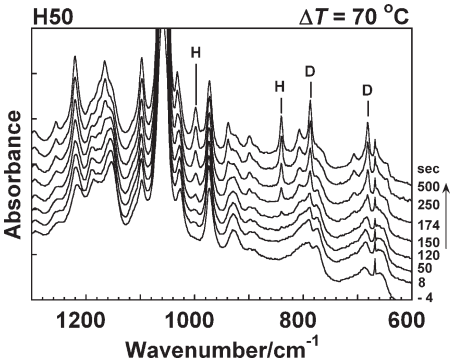

Figure 15. Time dependence of infrared spectra measured in the isothermal crystallization process of iPP H50 blend sample at ΔT = 70 °C.

the short helices are generated in the amorphous sea, and they grow in amount and length. They gather together locally and form isolated domains of 350−300 Å radius. These domains approach and correlate each other at about 300−250 Å distance while the helical segments further increase their lengths. This process further proceeds; finally, the stacked lamellar structure is formed with the long period of ca. 200 Å.

Cocrystallization. Figures 14 and 15 show the time dependence of infrared spectra measured at ΔT = 70 °C for H0 (pure D) and H50 (D/H blend) samples, respectively. For the H0 sample, we do not know the accurate critical sequence length for the infrared bands, although only one report was detected in a literature search.[42] By picking up some proper bands, we estimated the integrated intensity and compared their time dependence with the results of SAXS and WAXD analysis. Figures 16 and 17 show the results for H0 and H50 samples, respectively, where the time is on a logarithmic scale. In a similar manner, in the case of H100, the infrared bands corresponding to the regular helices start to grow in the early stage of crystallization. After that, the invariant, Q, and degree of crystallinity, X_c, increase with some decrement of long period. It should be noticed here that the D and H bands of the H50 blend sample start to be observed at almost the same time, although the pure H and D samples show largely different crystallization rates, as seen from the comparison of Figures 11 and 17. This clearly indicates the occurrence of the cocrystallization phenomenon between the D and H chains in the melt state. (From the comparison of the behavior of H and D IR bands, we might speculate that the D band at 678 cm^{-1} has the critical sequence length m = 10 and the 988 cm^{-1} D band has the

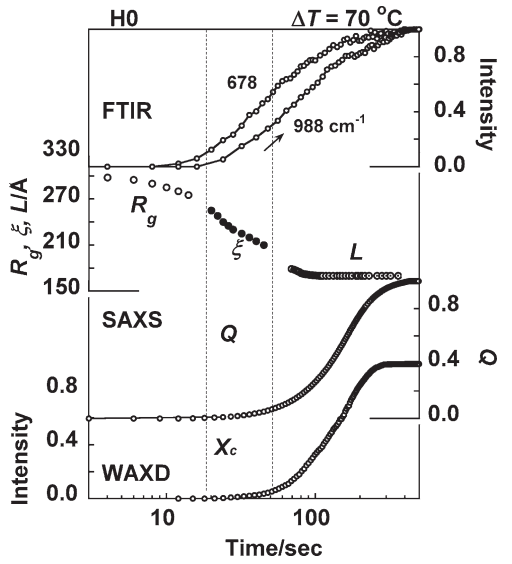

Figure 16. Comparison of infrared band intensity changes with the invariant Q and degree of crystallinity, X_c, and the long period, L, estimated for iPP H0 sample in the isothermal crystallization process (ΔT = 70 °C).

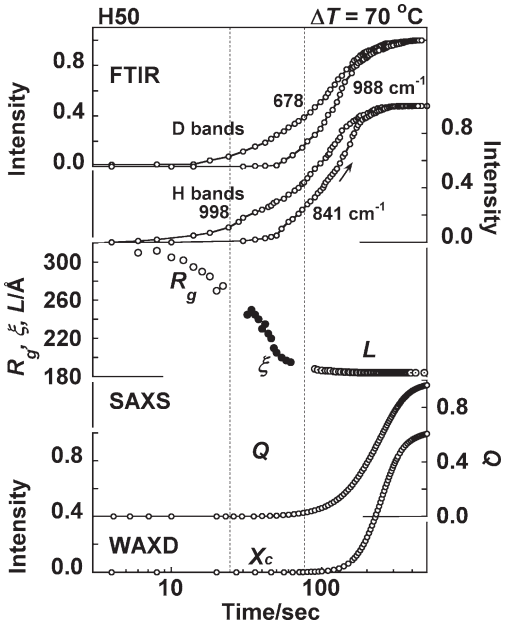

Figure 17. Comparison of infrared band intensity changes with the invariant, Q, and degree of crystallinity, X_c, and the long period, L, estimated for iPP H50 sample in the isothermal crystallization process (ΔT = 70 °C).

length m = 14.) As already pointed out, the crystallization rate of D species is originally much higher than that of H species.[34] If the diffusion motion of the chains controls the crystallization rate, then the faster migration results in the higher crystallization rate. If the isotopic fractionation occurs in the front-site region of the growing nuclei, then the faster D chains reach the site at first and attach to the crystalline site to grow. The H chains still remain in the melt, and the D/H content is changed there. With the passage of time, this process goes on, and the phase segregation might occur as a result. Figure 17 denies this possibility: the D and H chains reach the growing front site at almost the same time and give the intensity increment of helical infrared bands intrinsic to these species. Figure 18 shows these two different cases.

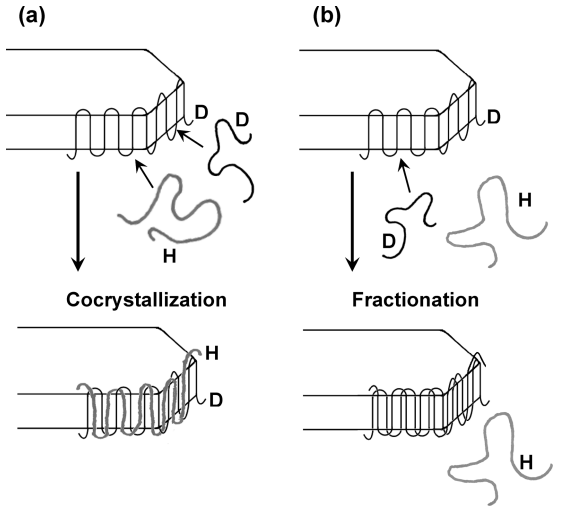

Figure 18. Schematic illustration of growing process occurring in the front site of a crystalline nucleus. (a) The diffusion rates of the H and D chains are almost the same, and the cocrystallization occurs. (b) The diffusion rate of the D chains is much higher than that of the H chains, resulting in the isotope fractionation and the phase segregation between these two species.

Conclusions

In the present article, we have discussed the isothermal crystallization behavior for a series of H/D blend samples of iPP by measuring the time-resolved synchrotron WAXD/SAXS and FTIR spectra, from which the detailed structural evolution process has been deduced in a concrete manner. In the early stage of crystallization, the regular but short helical segments start to appear and form an isolated domain in the molten amorphous sea. The SAXS data in this early stage were analyzed using a Guinier plot. As the number of regular and longer helical segments is increased, these domains start to show some degree of correlation to each other as they are analyzed reasonably on the basis of the Debye−Bueche theory. The transition from Guinier to Debye−Bueche regions or the transformation from R_g to ξ can be made smoothly. Around the time region of 300 s (for H 100 case at ΔT 70 °C), the stacked lamellar structure starts to form with a long period of ca. 200 Å, and they increase the volume with time.

In the case of the D/H blend sample, the formation of regular helical segments is observed to occur at almost the same time, indicating that the concept of isotopic fractionation near the growing front site is difficult to apply to this case. We need to investigate the difference in diffusion rate and the intermolecular interactions of the H and D chains in the melt for more discussion about the origin of D/H cocrystallization phenomenon.

Acknowledgment. This study was financially supported by a MEXT "Collaboration with Local Communities" project (2005−2009).

References and Notes

(1) A special issue on crystallization of polymers , *Faraday Discuss. Chem. Soc.* **1979**, *68*.
(2) *Proceedings of the NATO Advanced Research Workshops on Crystallization Process of Polymers*; Series C; Dasiere, M., Ed.; Kluwer Academic: Dordrecht, The Netherlands, **1993**; Vol. *405*.
(3) (a) Zhou, J. J.; Liu, J. G.; Yan, S. K.; Dong, J. Y.; Li, L.; Chan, C. M.; Schultz, J. M. *Polymer* **2005**, *46*, 4077. (b) Ryan, A. J.; Fairclough, J. P. A.; Terrill, N. J.; Olmsted, P. D.; Poon, W. C. K. *Faraday Discuss.* **1999**, *112*, 13. (c) Iijima, M.; Strobl, G. *Macromolecules* **2000**, *33*, 5204. (d) Heeley, E. L.; Maidens, A. V.; Olmsted, P. D.; Bras, W.;

Dolbnya, I. P.; Fairclough, J. P. A.; Terrill, N. J.; Ryan, A. J. *Macromolecules* **2003**, *36*, 3656. (e) Terrill, N. J.; Fairclough, P. A.; Towns-Andrews, E.; Komanschek, B. U.; Young, R. J.; Ryan, A. J. *Polymer* **1998**, *39*, 2381.
(4) (a) Kailas, L.; Vasilev, C.; Audinot, J. N.; Migeon, H. N.; Hobbs, J. K. *Macromolecules* **2007**, *40*, 7223. (b) Katzenberg, F.; Loos, J.; Petermann, J.; McMaster, T.; Miles, M. *Polym. Bull.* **1995**, *35*, 195. (c) Zia, Q.; Androsch, R.; Radusch, H. J.; Ingolic, E. *Polym. Bull.* **2008**, *60*, 791.
(5) (a) Clark, E. J.; Hoffman, J. D. *Macromolecules* **1984**, *17*, 878. (b) Martuscelli, E.; Pracella, M.; Crispino, L. *Polymer* **1983**, *24*, 693. (c) Maiti, P.; Hikasoka, M.; Yamada, K.; Toda, A.; Gu, F. *Macromolecules* **2000**, *33*, 9069. (d) Fatou, J. M. G.; Barrales-Lienda, J. M. *J. Polym. Sci., Part A: Polym. Chem.* **1969**, *7*, 175. (e) Blundell, D. J.; Beckett, D. R.; Willcocks, P. H. *Polymer* **1981**, *22*, 704.
(6) (a) Zhu, X. Y.; Yan, D. Y. *Macromol. Chem. Phys.* **2001**, *202*, 1109. (b) Zhu, X. Y.; Yan, D. Y.; Yao, H. X.; Zhu, P. F. *Macromol. Rapid Commun.* **2000**, *21*, 354.
(7) Wiochowicz, A.; Eder, M. *Polymer* **1981**, *22*, 1285.
(8) Hendra, P. J.; Vile, J.; Willis, H. A.; Zichy, V.; Cudby, M. E. A. *Polymer* **1984**, *25*, 785.
(9) (a) Konishi, T.; Nishida, K.; Kanaya, T. *Macromolecules* **2006**, *39*, 8035. (b) Ogino, Y.; Fukushima, H.; Takahashi, N.; Matsuba, G.; Nishida, K.; Kanaya, Y. *Macromolecules* **2006**, *39*, 7617.
(10) Tashiro, K.; Sasaki, S. *Prog. Polym. Sci.* **2003**, *28*, 451.
(11) Bruckner, S.; Meille, S. V.; Petraccone, V.; Pirozzi, B. *Prog. Polym. Sci.* **1991**, *16*, 361.
(12) Natta, G.; Corradini, P. *Nuovo Cimento Suppl.* **1960**, *15*, 40.
(13) Mencik, Z. *J. Macromol. Sci., Phys.* **1972**, *B6*, 101.
(14) Hikosaka, M.; Seto, T. *Polym. J.* **1973**, *5*, 111.
(15) Pae, K. D.; Sauer, J. A.; Morrow, D. R. *Nature* **1966**, *211*, 514.
(16) Tasumi, M.; Krimm, S. *J. Chem. Phys.* **1967**, *46*, 755.
(17) Tasumi, M.; Krimm, S. *J. Polym. Sci., Part A−2* **1968**, *6*, 995.
(18) Krimm, S.; Ching, J. H. C. *Macromolecules* **1972**, *5*, 209.
(19) Stehling, F. C.; Ergos, E.; Mandelkern, L. *Macromolecules* **1971**, *4*, 672.
(20) (a) Shelten, J.; Wignall, G. D.; Ballard, D. G. H. *Polymer* **1974**, *15*, 682. (b) Shelten, J.; Ballard, D. G. H.; Wignall, G. D.; Longman, G. W.; Schmatz, W. *Polymer* **1976**, *17*, 751. (c) Shelten, J.; Ballard, D. G. H.; Wignall, G. D.; Longman, G. W.; Schmatz, W. *Colloid Polym. Sci.* **1974**, *252*, 749. (d) Shelten, J.; Wignall, G. D.; Ballard, D. G. H.; Longman, G. W. *Polymer* **1977**, *18*, 1111.
(21) (a) Coutry, S.; Spells, S. J. *Polymer* **2002**, *43*, 4957. (b) Coutry, S.; Spells, S. J. *Polymer* **2003**, *44*, 1949. (c) Coutry, S.; Spells, S. J. *Polymer* **2006**, *47*, 3410.
(22) Tashiro, K.; Stein, R. S.; Hsu, S. L. *Macromolecules* **1992**, *25*, 1801.
(23) Tashiro, K.; Satkowski, M. M.; Stein, R. S.; Li, Y.; Chu, B.; Hsu, S. L. *Macromolecules* **1992**, *25*, 1809.
(24) Tashiro, K.; Izuchi, M.; Kobayashi, M.; Stein, R. S. *Macromolecules* **1994**, *27*, 1221.
(25) Tashiro, K.; Izuchi, M.; Kobayashi, M.; Stein, R. S. *Macromolecules* **1994**, *27*, 1228.
(26) Tashiro, K.; Izuchi, M.; Kobayashi, M.; Stein, R. S. *Macromolecules* **1994**, *27*, 1234.
(27) Tashiro, K.; Izuchi, M.; Kaneuchi, F.; Jin, C.; Kobayashi, M.; Stein, R. S. *Macromolecules* **1994**, *27*, 1240.
(28) Sasaki, S.; Tashiro, K.; Gose, N.; Imanishi, K.; Izuchi, M.; Kobayashi, M.; Imai, M.; Ohashi, M.; Yasuo, Y.; Ohayama, K. *Polym. J* **1999**, *31*, 677.
(29) Ballard, D. G. H.; Cheshire, P.; Longman, G. W.; Schelten, J. *Polymer* **1978**, *19*, 379.
(30) Ballard, D. G. H.; Longman, G. W.; Cowley, T. L.; Cunningham, A.; Schelten, J. *Polymer* **1979**, *20*, 399.
(31) Ballard, D. G. H.; Burgess, A. N.; Nevin, A.; Cheshire, P.; Longman, G. W.; Schelten, J. *Macromolecules* **1980**, *13*, 677.
(32) Kimata, S.; Sakurai, T.; Nozue, Y.; Kasahara, T.; Yamaguchi, N.; Karino, T.; Shibayama, M.; Kornfield, J. A. *Science* **2007**, *316*, 1014.
(33) Reddy, K. R.; Tashiro, K.; Sakurai, T.; Yamaguchi, N. *Macromolecules* **2008**, *41*, 9807.
(34) Reddy, K. R.; Tashiro, K.; Sakurai, T.; Yamaguchi, N. *Macromolecules* **2009**, *42*, 1672–1678.
(35) Hanna, L. A.; Hendra, P. J.; Maddams, W.; Willis, H. A.; Zichy, V.; Cudby, M. E. A. *Polymer* **1988**, *29*, 1843.
(36) (a) Tashiro, K.; Kobayashi, M.; Tadokoro, H. *Polym. J.* **1992**, *24*, 899. (b) Painter, P. C.; Watzek, M.; Koenig, J. L. *Polymer* **1977**, *18*, 1169.
(37) Zhu, X. Y.; Yan, D. Y.; Fang, Y. *J. Phys. Chem. B* **2001**, *105*, 12461.
(38) Zerbi, G.; Ciampelli, F.; Zamboni, V. *J. Polym. Sci.* **1963**, *C7*, 141.
(39) Kobayashi, M.; Akita, K.; Tadokoro, H. *Makromol. Chem.* **1968**, *118*, 324.
(40) Kissin, Y. V.; Tsvetkova, V. I.; Chirkov, N. M. *Vysokomol. Soedin.* **1968**, *A10*, 1092.
(41) Miyamoto, T.; Inagaki, H. *J. Polym. Sci.* **1969**, *A2*, 963.
(42) Kissin, Y. V.; Rishina, L. A. *Eur. Polym. J.* **1976**, *12*, 757.
(43) Kissin, Y. V. *Adv. Polym. Sci.* **1975**, *15*, 92.
(44) (a) Tashiro, K.; Ueno, Y.; Yoshioka, A.; Kobayashi, M. *Macromolecules* **2001**, *34*, 310. (b) Yoshioka, A.; Tashiro, K. *Macromolecules* **2003**, *36*, 3593. (c) Yoshioka, A.; Tashiro, K. *Macromolecules* **2004**, *37*, 467.
(45) (a) Tashiro, K.; Sasaki, S.; Kobayashi, M. *Macromolecules* **1996**, *29*, 7460. (b) Tashiro, K.; Sasaki, S.; Gose, N.; Kobayashi, M. *Polym. J.* **1998**, *30*, 485.
(46) (a) Tashiro, K.; Kobayashi, M.; Tadokoro, H. *Macromolecules* **1981**, *14*, 1757. (b) Tashiro, K.; Takano, K.; Kobayashi, M.; Chatani, Y.; Tadokoro, H. *Polymer* **1984**, *25*, 195. (c) Tashiro, K.; Kobayashi, M. *Polymer* **1988**, *29*, 4429.(d) Tashiro, K. Chapter 2. In *Ferroelectric Polymers*; Nalwa, H. S., Ed.; Marcel Dekker: New York, **1995**.(e) Asai, K.; Okamoto, M.; Tashiro, K. *Polymer* **2008**, *49*, 5186.
(47) Tashiro, K.; Imanishi, K.; Izuchi, M.; Kobayashi, M.; Kobayashi, K.; Satoh, M.; Stein, R. S. *Macromolecules* **1995**, *28*, 8477.
(48) Guinier, A.; Fournet, G. *Small Angle X-ray Scattering*; John Wiley & Sons, Inc.: London, **1955**.
(49) Akpalu, Y. A.; Amis, E. J. *J. Chem. Phys.* **1999**, *111*, 8686.
(50) Xiao, Z.; Akpalu, Y. A. *Polymer* **2007**, *48*, 5388.
(51) *Polymer Handbook*; Brandrup, J., Immergut, E. H., Grulke, E. A., Eds.; John Wiley & Sons, Inc.: Hoboken, NJ, **1999**; Vol. *1*.
(52) Debye, P.; Bueche, A. M. *J. Appl. Phys.* **1949**, *20*, 518.
(53) Strobl, G. R.; Schneider, M. *J. Polym. Sci., Polym. Ed.* **1980**, *18*, 1343.
(54) (a) Frohlich, H. *Theory of Dielectrics*, 2nd ed.; Clarendon: Oxford, U.K., **1960**. (b) Rothschild, W. G. Chapter 2. In *Band Shapes and Dynamics in Liquid in Vibrational Spectra and Structure*; During, J. R., Ed.; Elsevier: Amsterdam, **1986**; Vol. *15*.(c) Wang, C. H. *Spectroscopy of Condensed Media: Dynamics of Molecular Interactions*; Academic Press: New York, **1985**.(d) Choi, Y.; Kobayashi, M.; Tadokoro, H. *J. Chem. Phys.* **1986**, *84*, 4643.